

Reflect- and Transmit-Array Antennas for Scalable and Energy-Efficient mmWave Massive MIMO

Vahid Jamali, *Student Member, IEEE*, Antonia M. Tulino, *Fellow, IEEE*, Georg Fischer, *Senior Member, IEEE*, Ralf Müller, *Senior Member, IEEE*, and Robert Schober, *Fellow, IEEE*

Abstract—Hybrid analog-digital architectures are promising candidates for implementing millimeter wave (mmWave) massive multiple-input multiple-output (MIMO) systems since they enable a considerable reduction of the required number of costly radio frequency (RF) chains by moving some of the signal processing operations into the analog domain. Nevertheless, the analog feed network, comprising RF dividers, combiners, phase shifters, and line connections, of hybrid MIMO architectures is not scalable due to its prohibitively high power consumption for large numbers of transmit antennas. In this paper, we study novel massive MIMO architectures, namely reflect-array (RA) and transmit-array (TA) antennas, which consist of few active antennas (i.e., RF chains) and large numbers of passive antennas. We show that the constraints that the precoders for RA and TA antennas have to meet, differ from those of conventional MIMO architectures. Taking these constraints into account and exploiting the sparsity of mmWave channels, we design two efficient precoders for RA and TA antennas; one based on maximizing the mutual information and one based on approximating the optimal unconstrained digital precoder via the orthogonal matching pursuit algorithm. Furthermore, in order to fairly compare the performance of RA and TA antennas against conventional fully-digital and hybrid MIMO architectures, we develop a unified power consumption model. We study the impact of the system parameters on the achievable rate and show that a proper positioning of the active antennas with respect to the passive antennas in RA and TA MIMO leads to a considerable performance improvement. Our simulation results show that unlike conventional MIMO architectures, RA and TA antennas are highly energy efficient and fully scalable in terms of the number of transmit antennas. Therefore, RA and TA antennas are candidates for realizing the potential of *massive MIMO* in practice.

Index Terms—Reflect array, transmit array, hybrid MIMO, intelligent reflecting surfaces, mmWave communications, scalability, and energy efficiency.

I. INTRODUCTION

Millimeter wave (mmWave) communication systems are promising candidates to meet the high data rate demands of the next generation of wireless communication networks [2]–[4]. These systems are typically assumed to be equipped with a large array of antennas at the transmitter and/or the receiver to cope with the high path loss, limited scattering, and small antenna apertures at mmWave frequencies. However, conventional fully-digital (FD) multiple-input multiple-output (MIMO) systems, which connect each antenna to a dedicated radio frequency (RF) chain, are infeasible for mmWave systems

This paper has been accepted in part for presentation at IEEE ICC 2019 [1].

V. Jamali, R. Müller, and R. Schober are with the Institute for Digital Communications at Friedrich-Alexander University Erlangen-Nürnberg (FAU) (e-mail: vahid.jamali@fau.de; ralf.r.mueller@fau.de; robert.schober@fau.de).

A. M. Tulino is with Nokia Bell Labs, Holmdel, NJ 07733 USA, and also with the University degli Studi di Napoli Federico II, 80138 Naples, Italy (e-mail: a.tulino@nokia-bell-labs.com; antoniamaria.tulino@unina.it)

G. Fischer is with the Institute for Electronics Engineering at FAU (e-mail: georg.fischer@fau.de).

due to the prohibitively high cost and energy consumption of high resolution analog-to-digital/digital-to-analog converters needed per antenna element [2]. This has motivated researchers to consider hybrid analog-digital MIMO architectures, which tremendously reduce the required number of RF chains by moving some of the signal processing operations into the analog domain [3], [5]–[7].

Typically, in hybrid MIMO systems, it is assumed that the output of each RF chain is connected to all antennas. This architecture is referred to as fully-connected (FC) hybrid MIMO and is able to realize the full beamforming gain of massive antenna arrays. Unfortunately, FC hybrid MIMO is not scalable due to the excessive power consumption of the analog network for large numbers of antennas [8]. In particular, the analog network is comprised of RF dividers, combiners, phase shifters, and line connections, which lead to high RF losses and hence reduce energy efficiency. To deal with this issue, partially-connected (PC) hybrid MIMO architectures were proposed in the literature where the output of each RF chain is connected to only a subset of the antennas [2], [9]. Thereby, no RF combiner is needed, and the number of required phase-shifters and the required RF lines are reduced. Nevertheless, as will be shown in this paper, for PC hybrid MIMO, the power consumption still scales with the number of antennas in a similar manner as for FC hybrid MIMO.

In order to improve the scalability and energy-efficiency of mmWave massive MIMO systems, in this paper, we consider two novel massive MIMO architectures, namely reflect-array (RA) and transmit-array (TA) antennas, see Fig. 1. Both architectures comprise a large array of passive antenna elements and a few active antennas (also named illuminators which are usually horn antennas) [10]–[15]. Each active antenna is equipped with a dedicated RF chain and illuminates the array of passive antennas. Therefore, each passive element receives a superposition of the signals transmitted (over the air) by the active antennas and adds a desired phase shift to the overall signal. In RA, the phase-delayed signal is then reflected from the array whereas in TA, the phase-delayed signal is transmitted in the forward direction¹. Borrowing an analogy from optics, an RA is analogous to a curved mirror whereas a TA is analogous to a lens. The curvatures of this imagined mirror and lens are steerable via the phase shifters.

RA and TA antennas have been widely investigated in the microwave and antennas community and prototypes are available in the literature [10]–[15]. Thereby, the performance of

¹We note that RA and TA antennas have several advantages/disadvantages with respect to (w.r.t.) each other and which one is preferable depends on the particular implementation scenario. For instance, for RA antennas, the feed position introduces a blocking area whereas this issue does not exist for TA antennas. On the other hand, RA systems facilitate the placement of the control system for the phase shifters on the back side of the array [15].

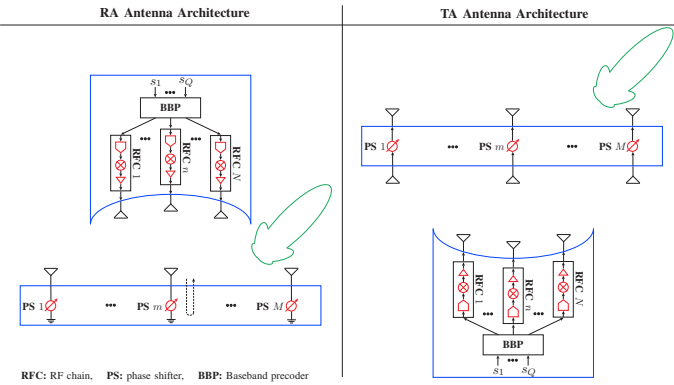


Fig. 1. Schematic illustration of the considered RA and TA massive MIMO architectures.

these architectures is typically characterized in terms of the beamforming gain. In contrast, in this paper, we are interested in multiplexing several data streams and the design of the corresponding precoder. In particular, this paper makes the following contributions:

- We first model the precoder structure of RA and TA antennas and show that the constraints they have to meet are different compared to those for conventional MIMO architectures. In addition, we simplify these constraints under the assumption of uniform illumination where the distribution of the power received from each active antenna at the passive antennas is uniform.
- Taking these constraints into account and exploiting the sparsity of mmWave channels, we design two efficient precoders for RA and TA antennas; one based on maximizing the mutual information (MI) and one based on approximating the optimal unconstrained FD precoder via orthogonal matching pursuit (OMP). The MI-based precoder yields a higher achievable rate compared to the OMP-based precoder at the expense of an increase in computational complexity.
- In order to conduct a fair comparison of the performance of RA and TA antennas and that of conventional MIMO architectures, we develop a unified power consumption model which includes the impacts of the loss over the air for the RA and TA architectures, the RF feed network for the FC and PC hybrid architectures, and the digital processing and power amplifiers for all architectures. This unified power model reveals that the power consumptions of the conventional MIMO architectures significantly increase as a function of the number of transmit antennas whereas the power consumptions of the RA and TA are almost independent of the number of transmit antennas.
- We study the impact of the system parameters on the achievable rate via simulation and show that a proper positioning of the active antennas w.r.t. the passive antennas in RA and TA MIMO leads to a considerable performance improvement. In addition, our simulation results show that in contrast to the conventional FD, FC, and PC MIMO architectures, the RA and TA MIMO architectures are highly energy-efficient and fully scalable in terms of the number of transmit antennas.

We note that the recent paper [16] also studied RA antennas where a precoder was designed based on alternating optimiza-

tion (AO). We employ this precoder as a benchmark and show that the proposed precoders outperform the AO-based precoder in [16] especially for environments with few scatterings. Moreover, the focus of this paper is mainly on the scalability and energy-efficiency of RA and TA MIMO systems which were not studied in [16]. Furthermore, compared to [16], in this paper, a more detailed model for the channel between the active and the passive antennas (which affects the precoder structure) is considered. Recent works [17]–[19] proposed to use intelligent reflecting surfaces (IRSs) or metasurfaces to enhance spectrum and energy efficiency in wireless communication networks. Similar to RA and TA antennas, IRSs employ a large number of passive elements each reflecting the incident signal with a certain phase shift to collaboratively achieve beamforming and/or interference suppression at designated receivers. Although both RA and TA antennas and IRSs employ passive antenna arrays, their structures are quite different. For example, for RA and TA antennas, the waves incident on the passive array come from physically close active antennas, where the channel between the active and passive antennas is fixed and can be properly designed during manufacturing. On the other hand, for IRSs, the waves incident on the passive array come from a transmitter which may be located far away, such that the channel between the transmitter and the passive array is subject to fading, cannot be influenced, and has to be estimated for beamforming design.

The rest of this paper is organized as follows. In Section II, we provide the system and power consumption models. The mathematical characterization of the RA and TA antenna architectures and the conventional MIMO architectures is presented in Section III. In Section IV, two different precoder designs for RA and TA antennas are developed. Simulation results are provided in Section V, and conclusions are drawn in Section VI.

Notations: Bold capital and small letters are used to denote matrices and vectors, respectively. $\|\mathbf{A}\|_F$, $\text{trace}(\mathbf{A})$, \mathbf{A}^T , and \mathbf{A}^H denote the Frobenius norm, trace, transpose, and Hermitian of matrix \mathbf{A} , respectively. $\mathbb{E}\{\cdot\}$ represents expectation and $I(\mathbf{x}; \mathbf{y})$ represents the MI between random variables (RVs) \mathbf{x} and \mathbf{y} . $|a|$ and $\angle a$ denote the absolute value and the angle of complex number a in polar coordinates, respectively. The big O notation $g(x) = O(f(x))$ indicates $\lim_{x \rightarrow \infty} |g(x)/f(x)| \leq k$ for some fixed $0 < k < \infty$. For a real number x , $[x]^+ = \max\{0, x\}$ and $[x]$ denotes the smallest integer number y for which $y \geq x$ holds. $\mathcal{CN}(\mu, \Sigma)$ denotes a complex normal RV with mean vector μ and covariance matrix Σ . Furthermore, $\mathbf{0}_n$ and $\mathbf{0}_{n \times m}$ denote a vector of size n and a matrix of size $n \times m$, respectively, whose elements are all zeros. \mathbf{I}_n is the $n \times n$ identity matrix and \mathbb{C} represents the set of complex numbers. $[a(m, n)]_{m,n}$ represents a matrix with element $a(m, n)$ in its m -th row and n -th column. $\mathbf{A}_{m,n}$ and \mathbf{a}_n denote the element in the m -th row and n -th column of matrix \mathbf{A} and the n -th element of vector \mathbf{a} , respectively. Finally, $\text{vec}(\mathbf{A})$ denotes a vector whose elements are the stacked columns of matrix \mathbf{A} .

II. SYSTEM, CHANNEL, SIGNAL, AND POWER CONSUMPTION MODELS

In this section, we present the adopted system and channel models as well as the signal and power consumption models.

A. System and Channel Models

We consider a point-to-point MIMO system where the transmitter and receiver have M and J antennas, respectively. The input-output MIMO model is given by

$$\mathbf{y} = \mathbf{H}\mathbf{x} + \mathbf{z}, \quad (1)$$

where $\mathbf{x} \in \mathbb{C}^{M \times 1}$ and $\mathbf{y} \in \mathbb{C}^{J \times 1}$ are the transmit and receive vectors, respectively. Moreover, $\mathbf{z} \in \mathbb{C}^{J \times 1}$ denotes the additive white Gaussian noise vector at the receiver, i.e., $\mathbf{z} \sim \mathcal{CN}(\mathbf{0}_J, \sigma^2 \mathbf{I}_J)$ where σ^2 denotes the noise variance at each receive antenna. Furthermore, $\mathbf{H} \in \mathbb{C}^{J \times M}$ is the channel matrix, which assuming the Saleh-Valenzuela model, is given by [9]

$$\mathbf{H} = \frac{1}{\sqrt{L}} \sum_{l=1}^L h_l \mathbf{h}_r(\theta_l^r, \phi_l^r) \mathbf{h}_t^H(\theta_l^t, \phi_l^t). \quad (2)$$

Here, L is the number of effective channel paths corresponding to a limited number of scatterers and $h_l \in \mathbb{C}$ is the channel coefficient of the l -th path. Moreover, $\mathbf{h}_t(\theta_l^t, \phi_l^t)$ ($\mathbf{h}_r(\theta_l^r, \phi_l^r)$) denotes the transmitter (receiver) antenna array response vector for elevation angle $\theta_l^t \in [0, \pi]$ ($\theta_l^r \in [0, \pi]$) and azimuth angle $\phi_l^t \in [0, 2\pi]$ ($\phi_l^r \in [0, 2\pi]$). For a uniform planar transmit array, we can obtain $\mathbf{h}_t(\theta_l^t, \phi_l^t)$ as [9]

$$\mathbf{h}_t(\theta_l^t, \phi_l^t) = \text{vec} \left(\left[e^{j \frac{2\pi d}{\lambda} ((m_1-1) \sin(\theta_l^t) \sin(\phi_l^t) + (m_2-1) \cos(\theta_l^t))} \right]_{m_1, m_2} \right), \quad (3)$$

where λ denotes the wavelength, and d is the distance between the array antenna elements. Assuming a square uniform planar array and that \sqrt{M} is integer, we have $m_1, m_2 = 1, \dots, \sqrt{M}$. For a uniform planar receiver array, $\mathbf{h}_r(\theta_l^r, \phi_l^r)$ can be analogous to $\mathbf{h}_t(\theta_l^t, \phi_l^t)$ in (3).

B. Transmit Signal and Power Consumption Models

Let $\mathbf{s} \in \mathbb{C}^{Q \times 1}$ denote the vector of Q independent data streams that we wish to transmit. Assuming linear precoding, the relation between \mathbf{x} and \mathbf{s} is as follows

$$\mathbf{x} = \sqrt{P_{\text{tx}}} \mathbf{F} \mathbf{s}, \quad (4)$$

where $\mathbf{F} \in \mathbb{C}^{M \times Q}$ is the precoder and P_{tx} denotes the transmit power. Here, we assume $\mathbb{E}\{\mathbf{s}\mathbf{s}^H\} = \mathbf{I}_Q$ and $\|\mathbf{F}\|_F = 1$. In this paper, we impose a constraint on the maximum power radiated from the passive array which is typically enforced by regulations. For example, for carrier frequencies 54-66 GHz, the United States Federal Communication Commissions (FCC) enforces a total maximum transmit power of 500 mW (27 dBm) for an emission bandwidth of more than 100 MHz [20]. Alternatively, one can impose a constraint on the power radiated from the active antennas². Although our derivations in Section III and the proposed precoder in Section IV are applicable for both power constraints, we focus on the former power constraint for RA and TA antennas since this enables a more straightforward comparison with the conventional MIMO architectures.

²The maximum radiated power is also constrained by the antenna effective isotropic radiated power (EIRP) [20]. The transmit power and EIRP are related according to $\text{EIRP} = G_{\text{max}} P_{\text{tx}}$, where G_{max} is the maximum antenna gain of the passive array.

In order to conduct a fair comparison between the power consumptions of the conventional MIMO architectures, i.e., FD, FC, and PC, and the considered MIMO architectures, i.e., RA and TA, a power consumption model that accounts for digital baseband processing, the RF network, and the power amplifiers is needed.

Baseband Circuitry: The circuit power consumption comprises the power consumed for baseband processing, denoted by P_{bb} , and by each RF chain (including the digital-to-analog converter, local oscillator, and mixer), denoted by P_{rfc} . Note that although, in principle, P_{bb} may vary as a function M , in the remainder of this paper, we assume P_{bb} is constant since its impact is typically much smaller than that of P_{rfc} [21], [22].

RF Network: For the FC and PC hybrid architectures, we assume an RF network with passive phase shifters, dividers, and combiners which introduce an insertion loss. For large RF networks, the insertion loss may easily exceed 20-30 dB which makes a one-shot power compensation infeasible due to amplifier nonlinearities at high gains [8]. In practice, to compensate for this insertion loss, multiple gain-compensation amplifiers (GCAs) are cascaded to ensure that a minimum power is delivered to drive the power amplifiers (PAs) before transmission via the antennas [8], [23]. Let G_{amp} denote the maximum amplification gain of the GCAs in dB, P_{amp} its respective power consumption, and L_{rf} the total loss in dB occurring in the RF network. Then, assuming that the signal is amplified by GCAs before being fed to the PAs to compensate for the RF losses³, the number of required GCAs per antenna is given by $\lceil \frac{L_{\text{rf}}}{G_{\text{amp}}} \rceil$. The exact number of required GCAs depends on the specific RF network architecture, of course, see e.g. Section III and Table I.

Power Amplifiers: The power consumed by the PAs is commonly modeled as $P_{\text{rd}}/\rho_{\text{pa}}$ where P_{rd} is the radiated output power and ρ_{pa} denotes the power amplifier efficiency [8], [22]–[24]. Note that for conventional MIMO architectures, P_{rd} is identical to P_{tx} , whereas for RA and TA antennas, P_{rd} is the power radiated by the active antennas which is typically larger than the power P_{tx} radiated by the passive array due to losses incurred by the channel between the active and the passive antennas, cf. Section III-A for details.

In summary, the total power consumption, denoted by P_{tot} , is obtained as

$$P_{\text{tot}} = P_{\text{bb}} + N P_{\text{rfc}} + \left\lceil \frac{L_{\text{rf}}}{G_{\text{amp}}} \right\rceil M P_{\text{amp}} + \frac{P_{\text{rd}}}{\rho_{\text{pa}}}. \quad (5)$$

III. MATHEMATICAL CHARACTERIZATION OF VARIOUS MIMO ARCHITECTURES

In this section, we characterize the constraints that different MIMO systems impose on precoder matrix \mathbf{F} and the corresponding total power consumption P_{tot} as a function of M .

³In practice, multiple stages of power amplification have to be performed within the RF network to ensure that the signal power does not get too weak, see [8] for examples of multiple-stage power amplification. Our motivation for considering single-stage power amplification in this paper is two-fold. First, the exact design of multiple-stage amplification crucially depends on the specific system parameters, e.g., M, N, G_{amp} , and L_{rf} , and cannot be easily generalized. Second, since the number of required GCAs are larger for multiple-stage amplification, single-stage amplification constitutes a favorable choice for the hybrid MIMO architectures, which are considered as performance benchmark.

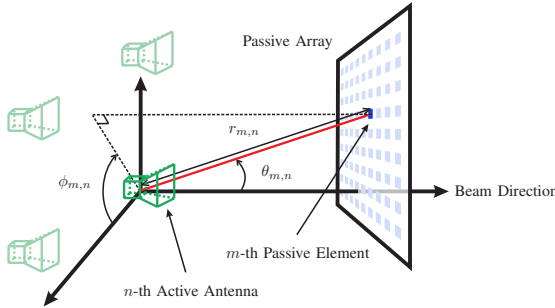


Fig. 2. Positioning of the active and passive antennas.

A. Reflect-Array and Transmit-Array

In the following, we first model the constraints that the RA and TA architectures impose on the precoder. Subsequently, we quantify the total power consumption of these architectures.

1) *Constraints on the Hybrid Precoder*: For the considered RA and TA architectures, we assume that each active feed antenna is connected to a dedicated RF chain, i.e., there are N active antennas. Moreover, we assume that the passive array comprises M antenna elements. To facilitate presentation, we characterize the positions of the passive antenna elements by $(r_{m,n}, \theta_{m,n}, \phi_{m,n})$, $r_{m,n} \geq 0$, $\theta_{m,n} \in [0, \pi]$, $\phi_{m,n} \in [0, 2\pi]$, in N different spherical coordinate systems corresponding to the locations of the active antennas and the direction of the beam such that each active antenna is the origin of one coordinate system and $\theta_{m,n}$ (elevation angle) is the angle between the beam and the line connecting the active antenna n to the passive element m , see Fig. 2 for an illustration of $(r_{m,n}, \theta_{m,n}, \phi_{m,n})$. Note that the values of $(r_{m,n}, \theta_{m,n}, \phi_{m,n})$ depend on the specific positioning of the feed antenna and the array antennas. Moreover, we make the following assumptions.

- A1) We assume the same antenna pattern for all active antennas with antenna gain $G(\theta, \phi)$ for elevation angle θ and azimuth angle ϕ . We further assume that the passive antennas have an isotropic antenna pattern.
- A2) We neglect the mutual coupling between active antennas and passive antennas, respectively, which is an accurate assumption when the antennas are sufficiently separated (typically $\lambda/2$). In addition, we assume that the passive array is in the far field of the active antennas which is valid if $r_{m,n} \gg \lambda$, $\forall m, n$ (typically $r_{m,n} \geq 5\lambda$, $\forall m, n$).
- A3) We assume that the power radiated from the active antennas is either reflected/forwarded or absorbed by the passive array such that no power from the active antennas directly arrives at the receiver.

Based on these assumptions, the following proposition quantifies the precoder structure for RA and TA antennas.

Proposition 1: Under assumptions A1-A3, the precoder \mathbf{F} for the RA and TA antennas has the form

$$\mathbf{F} = \mathbf{DTB}, \quad (6)$$

where $\mathbf{B} \in \mathbb{C}^{N \times Q}$ is the digital baseband precoder and $\mathbf{D} \in \mathbb{C}^{M \times M}$ is a diagonal matrix which controls the phase shifters and is obtained as

$$\mathbf{D} = \text{diag}(e^{j2\pi\beta_1}, \dots, e^{j2\pi\beta_M}) \quad (7)$$

with $\beta_m \in [0, 1]$. Moreover, $\mathbf{T} \in \mathbb{C}^{M \times N}$ is a fixed matrix which depends on the passive array power efficiency, denoted by ρ_{ary} , and the antenna positioning, namely $(r_{m,n}, \theta_{m,n}, \phi_{m,n})$, $\forall m, n$, and is given by

$$\mathbf{T} = \left[\frac{\lambda \sqrt{\rho_{\text{ary}} G(\theta_{m,n}, \phi_{m,n})}}{4\pi r_{m,n}} e^{-j\frac{2\pi r_{m,n}}{\lambda}} \right]_{m,n}. \quad (8)$$

Proof: The proof is given in Appendix A. ■

Proposition 1 shows that both RA and TA antennas have identical precoder structures, as given by (6). However, ρ_{ary} may assume different values for RA and TA antennas, see Section III-A2 for details. Therefore, the precoders that we develop in Section IV can be applied to both RA and TA antennas.

In the following, we consider a special case, which we refer to as *uniform illumination*. In particular, we make the following two assumptions to ensure a uniform power distribution across the passive antennas: *i*) We assume the distances between all pairs of active antennas and passive antennas are similar, i.e., $r_{m,n} \approx r$, $\forall m, n$, and *ii*) we assume a uniform feed antenna pattern $G(\theta_{m,n}, \phi_{m,n}) = G$, $\forall \theta \in [0, \theta_0]$, $\phi \in [0, 2\pi]$, where G is a constant and θ_0 is the elevation angular extent of the array w.r.t. the feed antenna. Based on these assumptions, the precoder is given in the following corollary.

Corollary 1: Under uniform illumination, matrix \mathbf{T} in (8) simplifies to

$$\mathbf{T} = \left[c e^{-j\frac{2\pi r_{m,n}}{\lambda}} \right]_{m,n} \quad \text{with} \quad c = \frac{\lambda}{4\pi r} \sqrt{\frac{2\rho_{\text{ary}}}{1 - \cos(\theta_0)}}. \quad (9)$$

Proof: The proof follows directly from noting that $G = \frac{2}{1 - \cos(\theta_0)}$ has to hold such that $\int_{\Omega} \frac{1}{4\pi} G(\phi, \theta) d\Omega = 1$ holds where $d\Omega = \sin(\theta) d\theta d\phi$ [25] and applying the simplifying assumption of uniform illumination in (6). ■

For single-stream data transmission, non-uniform illumination causes a decrease in the achievable antenna gain, which is known as taper loss [25, Chapter 15]. More generally, for multi-stream data transmission, non-uniform illumination reduces the achievable rate. We discuss taper loss further in the following subsection and study its impact via simulation in Section V.

2) *Power Consumption and Losses*: We assume passive arrays for the RA and TA architectures, i.e., no GCA is used. Nevertheless, we have several power losses due to propagation over the air and other inefficiencies which are discussed in detail in the following:

Spillover loss: Since the effective area of the array is finite, some of the power radiated by the active antennas will not be captured by the passive antennas, resulting in a spillover loss [11]. We define the efficiency factor ρ_S to take the spillover into account.

Taper loss: In general, the density of the received power differs across the passive antennas as they have different values for $G(\theta_{m,n}, \phi_{m,n})$ and $r_{m,n}$. As discussed earlier, for multi-stream transmission, taper loss leads to a reduction of the achievable rate. We define the efficiency factor ρ_T to account for this loss.

Aperture loss: Ideally, for RA antennas, the total power captured by the aperture will be reflected. In practice, however, a certain fraction of the captured power may be absorbed by the

RA. Similarly, for TA antennas, the aperture may not be able to fully forward the captured power and some of the power may be reflected in the backward direction or be absorbed by the TA. The aperture power efficiency is taken into account by introducing the efficiency factor ρ_A .

Phase shifters: Each phase shifter introduces a certain loss which is captured by the efficiency factor ρ_P . For TA antennas, the received signal passes through a phase shifter once before being forwarded whereas for RA antennas, the signal passes through a phase shifter twice before being reflected, see Fig. 1. Hence, the overall phase shifter efficiency factors for RA and TA antennas are ρ_P^2 and ρ_P , respectively.

It is well known that there is a trade-off between the spillover and taper losses such that the former can be decreased at the expense of increasing the latter by employing a narrower beam for the active antennas [25, Chapter 15]⁴. Note that the impacts of the spillover and taper losses are included in matrix \mathbf{T} in (8). Therefore, the array efficiency for RA and TA antennas is obtained as $\rho_{ary} = \rho_P^2 \rho_A$ and $\rho_{ary} = \rho_P \rho_A$, respectively, which accounts for the combined effects of the aperture and phase shifter losses. The transmit power is $\mathbb{E}\{\mathbf{x}^H \mathbf{x}\} = P_{tx} \|\mathbf{F}\|_F^2 = P_{tx}$ where $\mathbf{x} = \sqrt{P_{tx}} \mathbf{F} \mathbf{s}$ and $\|\mathbf{F}\|_F = 1$ whereas the power radiated by the active antennas is $P_{rd} = \mathbb{E}\{\bar{\mathbf{x}}^H \bar{\mathbf{x}}\} = P_{tx} \|\mathbf{B}\|_F^2$ where $\bar{\mathbf{x}} = \sqrt{P_{tx}} \mathbf{B} \mathbf{s}$ is the signal transmitted over the active antennas. In fact, due to the aforementioned power losses⁵, i.e., ρ_S , ρ_P , and ρ_A , the power radiated by the active antennas P_{rd} is not identical to the power radiated by the passive antennas P_{tx} . In summary, the total power consumption of the RA and TA MIMO architectures is obtained as

$$\begin{aligned} P_{tot} &= P_{bb} + NP_{rfc} + \frac{P_{tx} \|\mathbf{B}\|_F^2}{\rho_{pa}} \\ &\stackrel{(a)}{\approx} P_{bb} + NP_{rfc} + \frac{P_{tx}}{\rho_{rta} \rho_{pa}}, \end{aligned} \quad (10)$$

where $\rho_{rta} = \rho_S \rho_{ary}$ and approximation (a) holds assuming matrix \mathbf{T} is not ill conditioned, see Section V for further details. As can be seen from (10), the total power consumption of the RA and TA antennas does not explicitly change with increasing number of passive antennas M which makes them energy-efficient and scalable. Nevertheless, the values of ρ_S and ρ_T are determined by factors such as the size of the passive array, the beam pattern of the active antennas, the distance between the active antennas and the passive array, etc., which may in turn be influenced by M . In the following, we show for a simple example that ρ_S and ρ_T can be made independent of M by proper positioning of the antennas.

3) *Special Case:* To illustrate the variation of the spillover and taper losses as a function of the feed pattern and the angular extent of the antenna array, we consider the following simple class of axisymmetric feed antenna patterns which has been widely-adopted by the antenna community [11], [25]

$$G(\theta, \phi) = \begin{cases} 2(\kappa + 1) \cos^\kappa(\theta), & \text{if } 0 \leq \theta \leq \frac{\pi}{2} \\ 0, & \text{if } \frac{\pi}{2} < \theta \leq \pi, \end{cases} \quad (11)$$

⁴A similar behavior exists in the design of band-limited filters where there is a trade-off between the power leakage to adjacent frequency bands and the uniformity of the power distribution within the desired band [26].

⁵Note that taper loss reduces the achievable rate but does not constitute a power loss.

where $\kappa \geq 2$ is a real number and normalization factor $2(\kappa + 1)$ ensures that $\int_{\Omega} \frac{1}{4\pi} G(\phi, \theta) d\Omega = 1$ holds [25]. For this antenna pattern and assuming a *circular* planar array where the feed antenna orthogonally illuminates the center of the array, the spillover loss is obtained as [25, Chapter 15]

$$\rho_S = \frac{\int_{\phi} \int_{\theta=0}^{\theta_0} G(\phi, \theta) d\Omega}{\int_{\phi} \int_{\theta=0}^{\pi} G(\phi, \theta) d\Omega} = 1 - \cos^{\kappa+1}(\theta_0), \quad (12)$$

where θ_0 is the elevation angular extent of the array w.r.t. the feed antenna. Similarly, the taper loss is obtained as [25, Chapter 15]

$$\begin{aligned} \rho_T &= \frac{\left[\int_{\phi} \int_{\theta=0}^{\theta_0} \sqrt{G(\phi, \theta)} dS \right]^2}{2\pi(\cos^{-1}(\theta_0) - 1) \int_{\phi} \int_{\theta=0}^{\pi} G(\phi, \theta) dS} \\ &= \frac{\kappa - 1}{(\kappa/2 - 1)^2} \times \frac{\left[1 - \cos^{\kappa/2-1}(\theta_0) \right]^2}{(1 - \cos^{\kappa-1}(\theta_0))(\cos^{-1}(\theta_0) - 1)}, \end{aligned} \quad (13)$$

where $dS = dS_{\theta} dS_{\phi}$ is the normalized unit area covered by $[\theta, \theta + d\theta]$ and $[\phi, \phi + d\phi]$ on the antenna array where $dS_{\theta} = \cos^{-2}(\theta) d\theta$ and $dS_{\phi} = \sin(\theta) d\phi$. Moreover, the normalization factor $2\pi(\cos^{-1}(\theta_0) - 1)$ ensures that $\rho_T = 1$ for uniform illumination. Note that choosing larger κ decreases the spillover loss; however, it increases the taper loss.

The spillover and taper efficiencies in (12) and (13), respectively, were derived for circular planar arrays. For square planar arrays, we can obtain approximate expressions for ρ_S and ρ_T from (12) and (13), respectively, by approximating the square array with a circular array with the same area. In particular, for a square array with area $(\sqrt{M}d)^2$, the elevation angular extent θ_0 of its approximate circular array is obtained as

$$\theta_0 \approx \tan^{-1} \left(\frac{d}{R_d} \sqrt{\frac{M}{\pi}} \right), \quad (14)$$

where R_d is the distance between the active antenna and the passive antenna array. Therefore, for square arrays, if R_d is chosen to be proportional to \sqrt{M} , the value of θ_0 is independent of M . Hence, in this case, the spillover and taper losses do not scale with M .

B. Conventional MIMO Architectures

In the following, we study the precoder structure and power consumption of the conventional FD, FC, and PC MIMO architectures.

1) *Fully-Digital MIMO Architectures:* Here, we have $N = M$ RF chains which enable FD precoding, i.e., $\mathbf{F} = \mathbf{B}$ where \mathbf{B} is referred to as the digital precoder. Moreover, since we do not have an analog RF network, we obtain $L_{rf} = 0$ dB. Therefore, the total consumed power is given by

$$P_{tot} = P_{bb} + MP_{rfc} + \frac{P_{tx}}{\rho_{pa}}. \quad (15)$$

2) *Fully-Connected Hybrid MIMO Architectures:* In the FC hybrid architecture, we have N RF chains whose outputs are connected to all M antennas via analog dividers, phase shifters, and combiners. Typically, the relation $Q \leq N \ll M$ holds. For this MIMO architecture, the precoder has structure

$$\mathbf{F} = \mathbf{R} \mathbf{B}, \quad (16)$$

where $\mathbf{B} \in \mathbb{C}^{N \times Q}$ denotes the digital precoder and $\mathbf{R} \in \mathbb{A}^{M \times N}$ represents the analog RF precoder where $\mathbb{A} = \{x|x \in \mathbb{C} \text{ and } |x| = 1\}$. Based on the model introduced in Section II-B, we need to determine how many GCAs are needed to compensate the losses incurred in the RF network.

- *Dividers:* At the output of each RF chain, we need an $(M + 1)$ -port divider to feed all the antennas, i.e., one input and M outputs [23], [27]. Note that for input signal w , an ideal passive $(M + 1)$ -port power divider creates M output signals $\frac{1}{\sqrt{M}}w$ such that the sum of the powers of the output signals is identical to the power of the input signal. Nevertheless, in addition to factor $\frac{1}{\sqrt{M}}$, each power divider introduces a certain static power loss which should be taken into account. Assuming that these dividers are implemented as a cascade of simple three-port dividers, we need at least $\lceil \log_2(M) \rceil$ stages of division. Therefore, the overall loss at the output of the divider network is $\lceil \log_2(M) \rceil L_D$ where L_D is the power loss of each three-port divider in dB [23], [27]. Note that for an ideal divider with zero static loss, we obtain $L_D = 3$ dB.
- *Combiners:* Before being fed to an antenna, the RF signals from all RF chains have to be combined. Therefore, we need an $(N + 1)$ -port combiner for each antenna, i.e., N inputs and one output [23], [27]. For an ideal $(N + 1)$ -port combiner with input signals w_1, \dots, w_N , one may expect the output signal $w_1 + \dots + w_N$. However, for a passive combiner, at best $\frac{1}{\sqrt{N}}(w_1 + \dots + w_N)$ is realizable [27, Chapter 7]. Hereby, if all the input signals have the same phase and amplitude, the sum of the powers of the input signals is identical to the power of the output signal. Otherwise, there is a power loss which is referred to as dynamic power loss. Note that in reality, the output signals of the RF chains are random and a dynamic power loss of $\frac{1}{\sqrt{N}}$ is unavoidable. In addition to this dynamic power loss, each power combiner may introduce a certain static power loss. Implementing an $(N + 1)$ -port combiner based on the standard three-port combiners, we require at most $\lceil \log_2(N) \rceil$ stages of combining. Therefore, the overall loss at the output of the combiner network is $\lceil \log_2(N) \rceil L_C$ where L_C is the power loss of each three-port combiner in dB [23], [27]. Similar to an ideal divider, for an ideal combiner with zero static loss, we obtain $L_C = 3$ dB.
- *Phase Shifters:* As discussed earlier, each phase shifter may also introduce a static power loss, denoted by $L_P = 10 \log_{10}(1/\rho_P)$ [23], [27].

In summary, the total power consumption of the FC hybrid MIMO architecture is obtained as

$$\begin{aligned} P_{\text{tot}} = & P_{\text{bb}} + N P_{\text{rfc}} + \frac{P_{\text{tx}}}{\rho_{\text{pa}}} \\ & + \left\lceil \frac{[\log_2(M)] L_D + [\log_2(N)] L_C + L_P}{G_{\text{amp}}} \right\rceil M P_{\text{amp}}. \end{aligned} \quad (17)$$

3) *Partially-Connected MIMO Architectures:* As can be seen from (17), a huge challenge for the FC hybrid structure is scalability w.r.t. the number of antennas M . To address this issue, the PC hybrid MIMO structure has been proposed in the literature [9], [28]. The signal model for the PC architecture is identical to that in (16), i.e., $\mathbf{F} = \mathbf{RB}$, with the difference that

\mathbf{R} is now a block-diagonal matrix

$$\mathbf{R} = \begin{bmatrix} \mathbf{r}_1 & \mathbf{0}_{r_1} & \cdots & \mathbf{0}_{r_1} \\ \mathbf{0}_{r_2} & \mathbf{r}_2 & \cdots & \mathbf{0}_{r_2} \\ \vdots & \vdots & \ddots & \vdots \\ \mathbf{0}_{r_N} & \mathbf{0}_{r_N} & \cdots & \mathbf{r}_N \end{bmatrix}, \quad (18)$$

where $\mathbf{r}_n \in \mathbb{A}^{r_n \times 1}$ is the RF precoder vector which connects the output of the n -th RF chain to r_n antennas, and $\mathbf{0}_n$ is a vector of length n with all elements being equal to one. Note that $\sum_{n=1}^N r_n = M$ has to hold. In the simplest case, all RF chains are connected to the same number of antennas, i.e., $r_n = M/N, \forall n$, where we assume that N is a divisor of M .

Assuming again that power dividers are implemented as a cascade of simple three-port dividers, we need at least $\lceil \log_2(M/N) \rceil$ stages of division. Therefore, the overall loss at the output of the divider network is $\lceil \log_2(M/N) \rceil L_D$ [23], [27]. The passive phase shifters introduce an additional loss of L_P dB. Note that the PC architecture does not include a power combiner. In summary, the total power consumption for the PC MIMO architecture is given by

$$\begin{aligned} P_{\text{tot}} = & P_{\text{bb}} + N P_{\text{rfc}} + \frac{P_{\text{tx}}}{\rho_{\text{pa}}} \\ & + \left\lceil \frac{[\log_2(M/N)] L_D + L_P}{G_{\text{amp}}} \right\rceil M P_{\text{amp}}. \end{aligned} \quad (19)$$

C. Comparison

The constraints imposed on the precoder and the total power consumption of the different MIMO architectures discussed in this paper are summarized in Table I. As can be seen from this table, the total power consumption of all conventional massive MIMO architectures is increasing with the number of antennas M whereas the total power consumption of the RA and TA architectures does not scale with M . This illustrates the scalability of these architectures for large numbers of antennas.

IV. PRECODING DESIGN

In this section, we propose two linear precoders for RA and TA antennas exploiting the sparsity of the mmWave channel. We assume that the knowledge of channel state information (CSI) \mathbf{H} is available at the transmitter and is used for precoder design. Therefore, similar to the precoder designs in [3], [5]–[7], [16], [29], the frequency with which the proposed precoders (including the phase shifters of the passive array) have to be updated should be chosen based on the channel coherence time. This is in contrast to load modulated arrays [30] and media-based modulation [31] where antenna loads or phase shifters change at the symbol rate. Having the CSI, we ideally would like to design the optimal precoder which maximizes the achievable rate, $R(\mathbf{F}) \triangleq I(\mathbf{s}; \mathbf{y}) = \log_2 |\mathbf{I}_J + \gamma \mathbf{H} \mathbf{F} \mathbf{F}^H \mathbf{H}^H|$, based on

$$\begin{aligned} & \underset{\mathbf{F} \in \mathcal{F}}{\text{maximize}} \log_2 |\mathbf{I}_J + \gamma \mathbf{H} \mathbf{F} \mathbf{F}^H \mathbf{H}^H| \\ & \text{C1: } \|\mathbf{F}\|_F^2 \leq 1, \end{aligned} \quad (20)$$

where $\gamma = \frac{P_{\text{tx}}}{\sigma^2}$, C1 enforces the transmit power constraint, and \mathcal{F} is the set of feasible precoders which depends on the adopted MIMO architecture. For instance, for FC hybrid MIMO, we

TABLE I
COMPARISON OF DIFFERENT MIMO ARCHITECTURES, NAMELY FD, FC, PC, RA, AND TA.

Architecture	Precoder \mathbf{F}	Constraints	Total Power Consumption P_{tot}
FD	B	$\mathbf{B} \in \mathbb{C}^{M \times Q}$	$P_{\text{bb}} + M P_{\text{rfc}} + \frac{P_{\text{tx}}}{\rho_{\text{pa}}}$
FC	RB	$\mathbf{B} \in \mathbb{C}^{N \times Q}, \mathbf{R} \in \mathbb{A}^{M \times N}$	$P_{\text{bb}} + N P_{\text{rfc}} + \lceil \frac{[\log_2(M)]L_D + [\log_2(N)]L_C + L_P}{C_{\text{amp}}} \rceil M P_{\text{amp}} + \frac{P_{\text{tx}}}{\rho_{\text{pa}}}$
PC	RB	$\mathbf{B} \in \mathbb{C}^{N \times Q}, \mathbf{R} = \text{diag}(\mathbf{r}_1, \dots, \mathbf{r}_N), \mathbf{r}_n \in \mathbb{A}^{r_n \times 1}, \sum_{n=1}^N r_n = M$	$P_{\text{bb}} + N P_{\text{rfc}} + \lceil \frac{[\log_2(M/N)]L_D + L_P}{C_{\text{amp}}} \rceil M P_{\text{amp}} + \frac{P_{\text{tx}}}{\rho_{\text{pa}}}$
RA & TA	DTB	$\mathbf{B} \in \mathbb{C}^{N \times Q}, \text{fixed matrix } \mathbf{T} \in \mathbb{C}^{M \times N} \text{ (cf. (8))}, \mathbf{D} = \text{diag}(d_1, \dots, d_M), d_m \in \mathbb{A}$	$P_{\text{bb}} + N P_{\text{rfc}} + \frac{P_{\text{tx}}}{\rho_{\text{pta}} \rho_{\text{pa}}}$

have $\mathcal{F} = \{\mathbf{F} = \mathbf{R}\mathbf{B} \mid \mathbf{B} \in \mathbb{C}^{N \times Q} \text{ and } \mathbf{R} \in \mathbb{A}^{M \times N}\}$. Unfortunately, problem (20) is not tractable for hybrid MIMO architectures (including the considered RA and TA) since set \mathcal{F} is not convex due to modulo-one constraint on the elements of the analog precoder, cf. (16), (18), and (6). To cope with this issue, we exploit the spatial sparsity characteristic of mmWave channels as is explained in the following.

A. Rationale Behind the Proposed Precoders

For the spatially sparse channel model introduced in (2), $\mathcal{H}_t = \{\mathbf{h}_t(\theta_l^t, \phi_l^t), \forall l = 1, \dots, L\}$ forms a vector space for the rows of \mathbf{H} . In addition, since $L \ll M$ and (θ_l^t, ϕ_l^t) is taken from a continuous distribution, the elements of \mathcal{H}_t are with probability one linearly independent [5]. Let \mathcal{H}_t^\perp denote the null space of \mathcal{H}_t . Thereby, any precoder $\mathbf{F} = \mathbf{F}_{\mathcal{H}_t} + \mathbf{F}_{\mathcal{H}_t^\perp}$ can be decomposed into matrix $\mathbf{F}_{\mathcal{H}_t}$ belonging to space \mathcal{H}_t and matrix $\mathbf{F}_{\mathcal{H}_t^\perp}$ belonging to space \mathcal{H}_t^\perp . The following lemma formally characterizes the impact of $\mathbf{F}_{\mathcal{H}_t}$ and $\mathbf{F}_{\mathcal{H}_t^\perp}$ on the cost function and the constraint in (20).

Lemma 1: For any given precoder \mathbf{F} , relations $R(\mathbf{F}) = R(\mathbf{F}_{\mathcal{H}_t})$ and $\|\mathbf{F}\|_F \geq \|\mathbf{F}_{\mathcal{H}_t}\|_F$ hold.

Proof: The proof follows from similar arguments as those provided in [3], [5]–[7], [29] for precoder design of MIMO systems. In particular, for the achievable rate $R(\mathbf{F})$, the precoder appears in the term $\mathbf{H}\mathbf{F} = \mathbf{H}\mathbf{F}_{\mathcal{H}_t} + \mathbf{H}\mathbf{F}_{\mathcal{H}_t^\perp}$. The elements of matrix $\mathbf{H}\mathbf{F}_{\mathcal{H}_t^\perp}$ are obtained based on the multiplications of the rows of \mathbf{H} and the columns of $\mathbf{F}_{\mathcal{H}_t^\perp}$. Moreover, the rows of \mathbf{H} belong to space \mathcal{H}_t whereas the columns of $\mathbf{F}_{\mathcal{H}_t^\perp}$ belong to space \mathcal{H}_t^\perp . Since \mathcal{H}_t and \mathcal{H}_t^\perp are orthogonal, we obtain $\mathbf{H}\mathbf{F}_{\mathcal{H}_t^\perp} = \mathbf{0}_{J,N}$. Therefore, $\mathbf{F}_{\mathcal{H}_t^\perp}$ does not impact the achievable rate in (20). Moreover, we have $\|\mathbf{F}\|_F^2 = \text{trace}(\mathbf{F}\mathbf{F}^H) = \text{trace}((\mathbf{F}_{\mathcal{H}_t} + \mathbf{F}_{\mathcal{H}_t^\perp})(\mathbf{F}_{\mathcal{H}_t} + \mathbf{F}_{\mathcal{H}_t^\perp})^H) = \text{trace}(\mathbf{F}_{\mathcal{H}_t}\mathbf{F}_{\mathcal{H}_t}^H + \mathbf{F}_{\mathcal{H}_t^\perp}\mathbf{F}_{\mathcal{H}_t^\perp}^H) = \|\mathbf{F}_{\mathcal{H}_t}\|_F^2 + \|\mathbf{F}_{\mathcal{H}_t^\perp}\|_F^2 \geq \|\mathbf{F}_{\mathcal{H}_t}\|_F^2$ where we used $\text{trace}(\mathbf{F}_{\mathcal{H}_t}\mathbf{F}_{\mathcal{H}_t}^H) = \text{trace}(\mathbf{F}_{\mathcal{H}_t^\perp}\mathbf{F}_{\mathcal{H}_t^\perp}^H) = 0$. This concludes the proof. ■

Motivated by the above results, we limit our attention to precoders of the form $\mathbf{F} = \mathbf{F}_{\mathcal{H}_t}$. More explicitly, \mathbf{F} is rewritten as

$$\mathbf{F} = \mathbf{H}_t \mathbf{C}, \quad (21)$$

where $\mathbf{H}_t = [\mathbf{h}_t(\theta_1^t, \phi_1^t), \dots, \mathbf{h}_t(\theta_L^t, \phi_L^t)] \in \mathbb{C}^{M \times L}$ and $\mathbf{C} \in \mathbb{C}^{L \times Q}$ contains the corresponding coefficients. The similarity of the structure of the optimal precoder in (21) and the hybrid precoder $\mathbf{F} = \mathbf{R}\mathbf{B}$ has motivated researchers to use the channel response vectors $\mathbf{h}_t(\theta_l^t, \phi_l^t)$ for the columns of \mathbf{R} [2]–[5]. Since \mathbf{R} has N columns (i.e., N RF chains), the hybrid precoder problem simplifies to choosing the best N columns of \mathbf{H}_t and the corresponding coefficients. Unfortunately, this concept is not directly applicable to the precoder in (6) because of its different structure. Hence, we rewrite (21) in a more useful form. Let us

divide the index set of the passive antennas $\{1, \dots, M\}$ into N mutually exclusive sets \mathcal{M}_n , $n = 1, \dots, N$. Thereby, (21) can be rewritten as

$$\mathbf{F} = \sum_{n=1}^N \mathbf{H}_t^{\mathcal{M}_n} \mathbf{C}, \quad (22)$$

where $\mathbf{H}_t^{\mathcal{M}_n} = \mathbf{I}_{\mathcal{M}_n} \mathbf{H}_t \in \mathbb{C}^{M \times L}$ and $\mathbf{I}_{\mathcal{M}_n} \in \{0, 1\}^{M \times M}$ is a diagonal matrix whose m -th diagonal entry is one if $m \in \mathcal{M}_n$ and zero otherwise. In other words, we have decomposed \mathcal{H}_t into N subspaces, denoted by $\mathcal{H}_t^{\mathcal{M}_n}$, $n = 1, \dots, N$, which have mutually exclusive non-zero supports and are fully characterized by $\mathbf{H}_t^{\mathcal{M}_n}$, $n = 1, \dots, N$, respectively. In a similar manner, let us rewrite the precoder in (6) as

$$\mathbf{F} = \sum_{n=1}^N \mathbf{D}^{\mathcal{M}_n} \mathbf{T}^{\mathcal{M}_n} \mathbf{B}, \quad (23)$$

where $\mathbf{D}^{\mathcal{M}_n} = \mathbf{I}_{\mathcal{M}_n} \mathbf{D} \in \mathbb{A}^{M \times N}$ and $\mathbf{T}^{\mathcal{M}_n} = \mathbf{I}_{\mathcal{M}_n} \mathbf{T} \in \mathbb{C}^{M \times N}$. Comparing (22) and (23) motivates us to choose $\mathbf{D}^{\mathcal{M}_n}$ such that $\mathbf{D}^{\mathcal{M}_n} \mathbf{T}^{\mathcal{M}_n}$ becomes similar to $\mathbf{H}_t^{\mathcal{M}_n}$. To do this, we have to address the following two challenges. First, since $\mathbf{D}^{\mathcal{M}_n}$ has only M/N non-zero elements and $\mathbf{H}_t^{\mathcal{M}_n}$ has ML/N non-zero elements, $\mathbf{H}_t^{\mathcal{M}_n}$ cannot be fully reconstructed via $\mathbf{D}^{\mathcal{M}_n} \mathbf{T}^{\mathcal{M}_n}$ as matrix $\mathbf{T}^{\mathcal{M}_n}$ is fixed. Hereby, we choose to reconstruct only one column of $\mathbf{H}_t^{\mathcal{M}_n}$ via $\mathbf{D}^{\mathcal{M}_n} \mathbf{T}^{\mathcal{M}_n}$. The unmatched columns of $\mathbf{D}^{\mathcal{M}_n} \mathbf{T}^{\mathcal{M}_n}$ are treated as interference. Fortunately, for $M \gg N$, the interference approaches zero due to channel hardening. Second, we have to choose which column of $\mathbf{H}_t^{\mathcal{M}_n}$ to reconstruct. In the following, we introduce two approaches, namely MI-based and OMP-based methods, to choose the best N columns of $\mathbf{H}_t^{\mathcal{M}_n}$. Note that the above precoder design effectively reduces the search space for the diagonal analog precoder \mathbf{D} from multi-dimensional continuous set $\mathbb{A}^{M \times 1}$ to the finite elements of sets $\mathcal{H}_t^{\mathcal{M}_n}$, $n = 1, \dots, N$, i.e., NL elements in total. Therefore, as typically $N, L \ll M$, one can adopt an exhaustive search over this reduced space to obtain the optimal (e.g., rate-maximizing) analog precoder \mathbf{D} for a given baseband precoder \mathbf{B} .

B. MI-based Precoder

For the MI-based precoder, we design the analog precoders $\mathbf{D}^{\mathcal{M}_n}$, $n = 1, \dots, N$, and the corresponding baseband precoder in an iterative manner, such that the MI expression in (20) is maximized [29]. In particular, the proposed precoder design consists of an inner loop and an outer loop. The outer loop involves N iterations where in the n -th iteration, we choose the best analog precoder $\mathbf{D}^{\mathcal{M}_n}$ and the corresponding baseband precoder, denoted by \mathbf{B}_n , in the inner loop. In particular, the inner loop involves L iterations where in the l -th iteration, we maximize the achievable rate by optimizing the baseband

precoder \mathbf{B} assuming $\mathbf{D}^{\mathcal{M}_n}$ is one of the elements of $\mathcal{H}_t^{\mathcal{M}_n}$. Therefore, we have to consider the following two problems:

Optimizing the Baseband Precoder: Here, we assume the analog precoder $\mathbf{D} = \sum_{n=1}^N \mathbf{D}^{\mathcal{M}_n}$ is given. Then, the optimization problem for finding the digital baseband precoder \mathbf{B} simplifies to

$$\begin{aligned} & \underset{\mathbf{B} \in \mathbb{C}^{N \times Q}}{\text{maximize}} \left| \mathbf{I}_J + \gamma \mathbf{H} \mathbf{C}_1 \mathbf{B} \mathbf{B}^H \mathbf{C}_1^H \mathbf{H}^H \right| \\ & \text{C1: } \text{trace} \left(\mathbf{C}_1 \mathbf{B} \mathbf{B}^H \mathbf{C}_1^H \right) \leq 1, \end{aligned} \quad (24)$$

where $\mathbf{C}_1 = \mathbf{D} \mathbf{T} \in \mathbb{C}^{M \times N}$. Let us define matrix $\tilde{\mathbf{H}} = \mathbf{H} \mathbf{C}_1 (\mathbf{C}_1^H \mathbf{C}_1)^{-\frac{1}{2}} \in \mathbb{C}^{J \times N}$ and its corresponding singular value decomposition (SVD) $\tilde{\mathbf{H}} = \mathbf{U} \Sigma \mathbf{V}^H$, where $\mathbf{U} = [\mathbf{u}_1, \dots, \mathbf{u}_J] \in \mathbb{C}^{J \times J}$ and $\mathbf{V} = [\mathbf{v}_1, \dots, \mathbf{v}_N] \in \mathbb{C}^{N \times N}$ are unitary matrices containing the left and right singular vectors, respectively, and Σ is a diagonal matrix containing the singular values $\sigma_1, \dots, \sigma_N$ in descending order. The solution of (24) is given in the following lemma.

Lemma 2: For a given analog precoder \mathbf{D} , the optimal baseband precoder \mathbf{B} as a solution of (24) is given by

$$\mathbf{B} = (\mathbf{C}_1^H \mathbf{C}_1)^{-\frac{1}{2}} [\mathbf{v}_1, \dots, \mathbf{v}_Q] \mathbf{Z}, \quad (25)$$

where $\mathbf{Z} = \text{diag}(\sqrt{z_1}, \dots, \sqrt{z_Q}) \in \mathbb{C}^{Q \times Q}$, $z_q = \left[\mu - \frac{1}{\gamma \sigma_q^2} \right]^+$, and threshold μ is chosen such that constraint $\sum_{q=1}^Q z_q = 1$ is met.

Proof: The proof is given in Appendix B. \blacksquare

Note that the baseband precoder \mathbf{B} effectively eliminates the interference between the data streams.

Optimizing the Analog Precoder: As discussed earlier, we decompose \mathbf{D} into N components $\mathbf{D}^{\mathcal{M}_n}$, $n = 1, \dots, N$, which are initialized to the identity matrix \mathbf{I}_M and their values are updated in each iteration. In particular, in the n -th iteration, the following problem is solved

$$\underset{\mathbf{D}^{\mathcal{M}_n} \in \mathcal{D}_n}{\text{maximize}} \left| \mathbf{I}_J + \gamma \mathbf{H} \mathbf{D}^{\mathcal{M}_n} \mathbf{C}_2 \mathbf{D}^{\mathcal{M}_n H} \mathbf{H}^H \right|, \quad (26)$$

where $\mathbf{C}_2 = \mathbf{T} \mathbf{B}(\mathbf{D}) \mathbf{B}(\mathbf{D})^H \mathbf{T}^H \in \mathbb{C}^{M \times M}$. Here, $\mathbf{B}(\mathbf{D})$ denotes the optimal baseband precoder as a function of a given analog precoder \mathbf{D} which is obtained from (25). Moreover, set \mathcal{D}_n is given by

$$\begin{aligned} \mathcal{D}_n = \left\{ \mathbf{D}^{\mathcal{M}_n}[l] \in \mathbb{A}^{M \times M}, \forall l = 1, \dots, L \mid \mathbf{D}_{m,m'}^{\mathcal{M}_n}[l] = \right. & \quad (27) \\ \left. \begin{cases} \exp \left(j \left[\angle(\mathbf{H}_t^{\mathcal{M}_n})_{m,l} - \angle \mathbf{T}_{m,n} \right] \right), & \forall m = m' \in \mathcal{M}_n \\ 0, & \text{otherwise} \end{cases} \right\}. \end{aligned}$$

As can be seen, the cardinality of \mathcal{D}_n is L which allows us to solve (26) via an exhaustive search. Algorithm 1 summarizes the above main steps for the proposed MI-based precoder design.

C. OMP-based Precoder

In this subsection, we propose a second precoder, namely the OMP-based precoder, which is computationally less complex than the MI-based precoder (cf. Section IV-D) but achieves a similar performance (cf. Section V). In particular, the OMP-based precoder attempts to approximate the optimal unconstrained precoder for the FD MIMO architecture, denoted by \mathbf{F}^{opt} , using the OMP algorithm. Minimization of $\|\mathbf{F}^{\text{opt}} - \mathbf{F}\|_F$ is commonly adopted in the literature as design criterion for

Algorithm 1 MI-based Precoder Design

```

1: initialize:  $\mathbf{D}^{\mathcal{M}_n} = \mathbf{I}_M, \forall n$ .
2: for  $n = 1, \dots, N$  do
3:   for  $l = 1, \dots, L$  do
4:     Set  $\mathbf{D}^{\mathcal{M}_n} = \mathbf{D}^{\mathcal{M}_n}[l]$  from  $\mathcal{D}_n$  in (27).
5:     Find  $\mathbf{B}[l]$  using (25) for  $\mathbf{D}[l] = \sum_{i=1}^n \mathbf{D}^{\mathcal{M}_i}$ .
6:     Set  $R[l] = \log_2 \left( \left| \mathbf{I}_J + \gamma \mathbf{H} \mathbf{F}^{\text{opt}} \mathbf{H}^H \right| \right)$  for  $\mathbf{F} = \mathbf{D}[l] \mathbf{T} \mathbf{B}[l]$ .
7:   end for
8:   Update  $\mathbf{D}^{\mathcal{M}_n} = \mathbf{D}^{\mathcal{M}_n}[l^*]$  and  $\mathbf{B}_n = \mathbf{B}[l^*]$  for  $l^* = \max_l R[l]$ .
9: end for
10: Return  $\mathbf{D} = \sum_{n=1}^N \mathbf{D}^{\mathcal{M}_n}$  and  $\mathbf{B} = \mathbf{B}_N$ .

```

constrained hybrid precoders [3], [5], [16], [22]. Motivated by this, we consider the following optimization problem for the RA and TA MIMO architectures

$$\begin{aligned} & \underset{\mathbf{B} \in \mathbb{C}^{N \times Q}, \mathbf{D}^{\mathcal{M}_n} \in \mathcal{D}_n}{\text{minimize}} \|\mathbf{F}^{\text{opt}} - \mathbf{D} \mathbf{T} \mathbf{B}\|_F^2 \\ & \text{C1: } \|\mathbf{D} \mathbf{T} \mathbf{B}\|_F^2 \leq 1. \end{aligned} \quad (28)$$

Again, let us fix sets \mathcal{M}_n , $n = 1, \dots, N$, a priori. The proposed precoder employs N iterations where in each iteration, the following two problems are solved:

Optimizing the Analog Precoder: Let $\mathbf{F}_n^{\text{res}} = \mathbf{F}^{\text{opt}} - \sum_{i=1}^n \mathbf{D}^{\mathcal{M}_i} \mathbf{T}^{\mathcal{M}_i} \mathbf{B}_n$ denote the residual precoder in iteration n where \mathbf{B}_n is the baseband precoder designed in iteration n . In each iteration, we project the residual matrix from the previous iteration onto the space defined by \mathbf{H}_t and find the direction l^* that has the maximum projected value. This can be mathematically formulated as

$$l_n^* = \underset{l=1, \dots, L}{\text{argmax}} (\Psi \Psi^H)_{l,l}, \quad (29)$$

where $\Psi = \mathbf{H}_t^H \mathbf{F}_{n-1}^{\text{res}} \in \mathbb{C}^{L \times Q}$. Therefore, $\mathbf{D}^{\mathcal{M}_n}$ is selected as the element of \mathcal{D}_n corresponding to l^* -th channel path, cf. (2).

Optimizing the Baseband Precoder: By defining $\mathbf{C}_3 = \sum_{i=1}^n \mathbf{D}^{\mathcal{M}_i} \mathbf{T}^{\mathcal{M}_i} \in \mathbb{C}^{M \times N}$, we can formulate the optimization problem for \mathbf{B}_n as

$$\begin{aligned} & \underset{\mathbf{B} \in \mathcal{B}}{\text{minimize}} \|\mathbf{F}^{\text{opt}} - \mathbf{C}_3 \mathbf{B}\|_F^2, \\ & \text{C1: } \|\mathbf{C}_3 \mathbf{B}\|_F^2 \leq 1, \end{aligned} \quad (30)$$

which has the following well-known normalized least square solution [5]

$$\mathbf{B}_n = \frac{(\mathbf{C}_3^H \mathbf{C}_3)^{-1} \mathbf{C}_3^H \mathbf{F}^{\text{opt}}}{\|\mathbf{C}_3 (\mathbf{C}_3^H \mathbf{C}_3)^{-1} \mathbf{C}_3^H \mathbf{F}^{\text{opt}}\|_F}. \quad (31)$$

Algorithm 2 summarizes the above main steps for the proposed OMP-based precoder design.

D. Complexity Analysis

Let us assume that $M \gg J \geq N \geq Q$ and $M \gg L \geq N \geq Q$ hold. Moreover, we use the following results: The SVD of matrix $\mathbf{A} \in \mathbb{C}^{m \times n}$ of rank p has complexity order $O(mnp)$, the inversion of matrix $\mathbf{A} \in \mathbb{C}^{m \times m}$ has complexity order $O(m^3)$, and the multiplication \mathbf{AB} of matrices $\mathbf{A} \in \mathbb{C}^{m \times n}$

Algorithm 2 OMP-based Precoder Design

```

1: initialize:  $\mathbf{F}_0^{\text{res}} = \mathbf{F}^{\text{opt}}$  and  $\mathbf{D}^{\mathcal{M}_n} = \mathbf{0}_{M \times M}$ ,  $\forall n$ .
2: for  $n = 1, \dots, N$  do
3:    $l_n^* = \text{argmax}_{l=1, \dots, L} (\Psi \Psi^H)_{l,l}$  for  $\Psi = \mathbf{H}_t^H \mathbf{F}_{n-1}^{\text{res}}$ .
4:   Update  $\mathbf{D}^{\mathcal{M}_n}$  as the element of set  $\mathcal{D}_n$  in (27) corresponding to  $l_n^*$ .
5:   Update  $\mathbf{B}_n$  using (31) for  $\mathbf{C}_3 = \sum_{i=1}^n \mathbf{D}^{\mathcal{M}_i} \mathbf{T}^{\mathcal{M}_i}$ .
6:   Update  $\mathbf{F}_n^{\text{res}} = \mathbf{F}^{\text{opt}} - \sum_{i=1}^n \mathbf{D}^{\mathcal{M}_i} \mathbf{T}^{\mathcal{M}_i} \mathbf{B}_n$ .
7: end for
8: Return  $\mathbf{D} = \sum_{n=1}^N \mathbf{D}^{\mathcal{M}_n}$  and  $\mathbf{B} = \mathbf{B}_N$ .

```

and $\mathbf{B} \in \mathbb{C}^{n \times p}$ has complexity order $O(mnp)$ [32]. The MI-based precoder involves NL iterations (i.e., inner and outer loops) where each iteration comprises the SVD of matrix $\tilde{\mathbf{H}}$ (i.e., $O(JN^2)$), the inversion of matrix $\mathbf{C}_1^H \mathbf{C}_1$ (i.e., $O(N^3)$), and matrix multiplications (i.e., $O(MNJ)$). Hence, recalling $M \gg J, N, Q$, the overall complexity order of the MI-based precoder is $O(MN^2JL)$. On the other hand, the OMP-based precoder requires the SVD of matrix \mathbf{H} (i.e., $O(MJL)$) and involves N iterations where each iteration comprises the inversion of matrix $\mathbf{C}_3^H \mathbf{C}_3$ (i.e., $O(N^3)$) and matrix multiplications (i.e., $O(MLQ + MN^2)$). Assuming $N = Q$, the overall complexity order of the OMP-based precoder simplifies to $O(M(N^2 + J)L)$. Therefore, computing the OMP-based precoder entails a lower complexity than computing the MI-based precoder.

V. SIMULATION RESULTS

In this section, we first describe the considered simulation setup. Subsequently, we study the performance of the proposed precoders and the impact of the system parameters. Finally, we compare the performances of the considered mmWave massive MIMO architectures.

A. Simulation Setup

We generate the channel matrices according to (2). Thereby, we assume that the angles θ_l^t , θ_l^r , ϕ_l^t , and ϕ_l^r are uniformly distributed RVs in the intervals $[0, \theta_l^t]$, $[0, \bar{\theta}_l^t]$, $[0, \bar{\phi}_l^t]$, and $[0, \bar{\phi}_l^r]$, respectively, and $\bar{\theta}_l^t$ and $\bar{\theta}_l^r$ ($\bar{\phi}_l^t$ and $\bar{\phi}_l^r$) are the elevation (azimuth) coverage angles of the transmitter and receiver antennas, respectively. Moreover, we use the square uniform planar array in (3), i.e., a $\sqrt{Md} \times \sqrt{Md}$ planar array. The channel coefficient for each effective path is modeled as $h_l = \sqrt{\bar{h}_l} \tilde{h}_l$ where \bar{h}_l and \tilde{h}_l are the path loss and the random fading components, respectively, and are given by

$$\bar{h}_l = \left(\frac{\lambda}{4\pi\ell} \right)^\eta \quad \text{and} \quad \tilde{h}_l = \mathcal{CN}(0, 1), \quad (32)$$

respectively. In (32), ℓ denotes the distance between the transmitter and the receiver and η represents the path-loss exponent. The noise power at the receiver is given by $\sigma^2 = WN_0N_F$ where W is the bandwidth, N_0 represents the noise power spectral density, and N_F denotes the noise figure.

We arrange the active antennas w.r.t. the array of passive antennas as shown in Fig. 3 and described in the following. All active antennas have distance R_d from the passive array and are uniformly located on a ring of radius R_r , see the left-hand

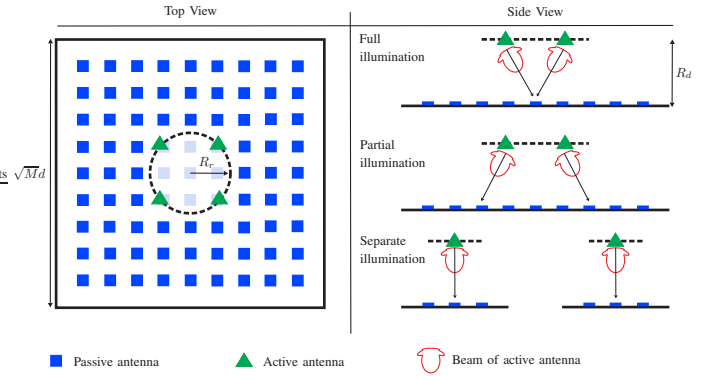


Fig. 3. Schematic illustration of the arrangement of the active and passive antennas and different illumination scenarios.

side of Fig. 3. Moreover, we adopt the feed antenna pattern in (11), which is widely used in the antenna community [11], [25]. In addition, we consider the following three illumination scenarios, see the right-hand side of Fig. 3:

- **Full illumination:** Similar to the setup in [16], we assume that each active antenna fully illuminates the passive array, referred to as full illumination (FI). To achieve this, we assume that all active antennas illuminate the center of the passive array.
- **Partial illumination:** Here, we assume that the passive antenna elements responsible for a given active antenna are physical neighbors and each active antenna illuminates the center of its respective passive antennas. Therefore, each active antenna mostly illuminates the subset of passive antenna elements allocated to it, which is referred to as partial illumination (PI). Our motivation for considering PI is that for the proposed precoder, only a part of the passive array is responsible for reflection/transmission of the signal received from a given active antenna.
- **Separate illumination:** Next, we assume that each active antenna and its respective passive antenna elements are physically separated/shielded from the other active and passive antennas. We refer to this setup as separate illumination (SI). In addition, we assume that each active antenna illuminates the center of its respective sub-array. Note that due to the wide beam patterns of the active antennas, even under PI, they illuminate not only their respective subset of passive antennas, but all other antenna elements as well. This causes interference between the signals from different RF chains which is avoided by SI.

In addition to the above three illumination scenarios, we also investigate the impact of uniform vs. non-uniform illumination, i.e., uniform vs. non-uniform power distribution across the passive antenna elements, cf. Proposition 1 and Corollary 1. Unless otherwise stated, the default values of the system parameters, including parameters R_r and R_d , for the aforementioned FI, PI, and SI are provided in Table II. All results shown in this section have been averaged over 10^3 random realizations of the channel matrix.

B. Performance of Proposed Precoders and Impact of the System Parameters

In Fig. 4, we show the spectral efficiency R (bits/s/Hz) from (20) versus the number of transmit antennas M for SI,

TABLE II
DEFAULT VALUES OF SYSTEM PARAMETERS [8], [13], [14], [22], [24].

Parameter	ℓ	η	$\bar{\theta}_l^r, \bar{\theta}_l^r$	$\bar{\phi}_l^r, \bar{\phi}_l^r$	L	N_0	N_F	W	λ	d	R_r	R_d	κ		
Value	100 m	2	$\pi/3$	$2\pi/3$	8	-174 dBm/Hz	6 dB	100 MHz	5 mm	$\lambda/2$	FI: $2d$, PI, SI: $\frac{4\sqrt{2M}}{4}$	FI: $\frac{d\sqrt{M}}{\sqrt{\pi}}$, PI, SI: $\frac{d\sqrt{M}}{\sqrt{4\pi}}$	6		
Parameter	P_{bb}	P_{rfc}	P_{tx}	P_{amp}	G_{amp}	L_D	L_C	L_P (1/ ρ_P in dB)		1/ ρ_A in dB	ρ_{amp}	Q	N	M	J
Value	200 mW	100 mW	20 dBm	40 mW	10 dB	3.6 dB	3.6 dB	2 dB		RA: 0.5 dB, TA: 1.5 dB	0.3	4	4	256	16

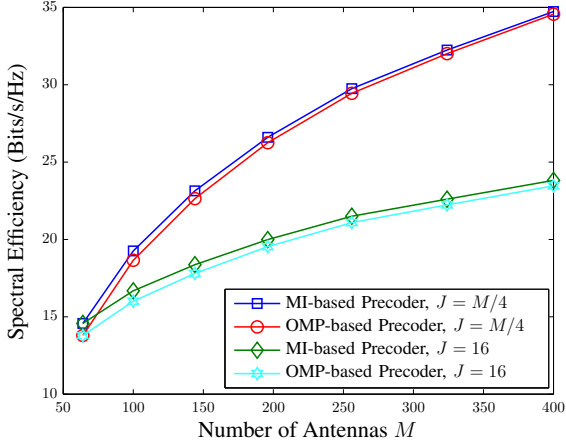


Fig. 4. Spectral efficiency (bits/s/Hz) versus number of transmit antennas M for SI, $P_{tx} = 20$ dBm, $Q = N = 4$, and $J \in \{16, M/4\}$.

$P_{tx} = 20$ dBm, $Q = N = 4$, and $J \in \{16, M/4\}$. Note that both RA and TA MIMO yield the same spectral efficiency since their only difference is the array efficiency factor ρ_A which influences their power consumption but does not impact their spectral efficiency. We observe that, as the number of antennas M increases, the spectral efficiency increases. However, the slope of the increase is larger for $J = M/4$ than for $J = 16$. As can be seen from Fig. 4, the MI-based precoder outperforms the OMP-based precoder in terms of spectral efficiency. This is expected since the MI-based precoder is optimized for maximization of the achievable rate whereas the OMP-based precoder is obtained by approximating the optimal unconstrained FD precoder. Nevertheless, the additional gain of the MI-based precoder is small and decreases as M increases. This can be attributed to the fact that both the MI- and OMP-based precoders search over the same sets for their respective analog precoders whose cardinality is rather small, i.e., NL . In summary, we can conclude that the OMP-based precoder has a comparable performance as the MI-based precoder but the complexity of Algorithm 2 for computing the OMP-based precoder is lower than that of Algorithm 1 for computing the MI-based precoder. Therefore, for the remainder of this section, we focus on the OMP-based precoder.

In Fig. 5, we show the spectral efficiency (bits/s/Hz) versus the number of transmit antennas M for $P_{tx} = 20$ dBm, $Q = N = 4$, $J = 16$, and different illumination scenarios, namely non-uniform FI, non-uniform PI, non-uniform SI, and uniform SI. As can be observed from this figure, PI achieves a considerable performance gain compared to FI. For the proposed precoder, this can be justified since each part of the passive array is responsible for reflection/transmission of the signal from one of the active antennas. Therefore, PI reduces

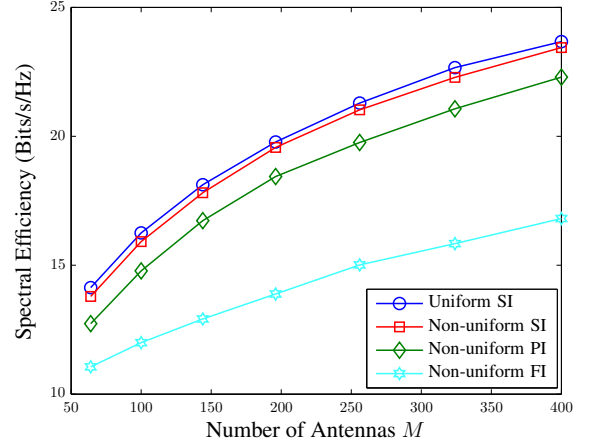


Fig. 5. Spectral efficiency (bits/s/Hz) versus number of transmit antennas M for $P_{tx} = 20$ dBm, $J = 16$, and different illumination scenarios.

the excessive interference that is caused by FI. Moreover, we observe that a further gain is achieved by SI compared to PI by completely avoiding this interference. To study the impact of the power distribution across the passive antennas, we show the achievable rate for SI for both non-uniform and uniform illumination, cf. Proposition 1 and Corollary 1. As expected uniform SI outperforms non-uniform SI; nevertheless, the additional gain is marginal.

Next, we study the impact of the positioning of the passive and active antennas via parameters R_r and R_d . An unfavorable positioning of the active and passive antennas causes matrix \mathbf{T} to be ill conditioned which in turn decreases the achievable rate of any precoder design due to the reduced degrees of freedom in $\mathbf{F} = \mathbf{DTB}$. Moreover, an ill-conditioned matrix \mathbf{T} leads to an increase of the power needed to be radiated by the active antennas to achieve a certain transmit power for the passive array. Therefore, as performance metric, we consider the condition number of matrix \mathbf{T} , denoted by $\varpi(\mathbf{T}) = \frac{\sigma_{\max}(\mathbf{T})}{\sigma_{\min}(\mathbf{T})}$, where $\sigma_{\max}(\mathbf{T})$ and $\sigma_{\min}(\mathbf{T})$ denote the maximum and minimum singular values of \mathbf{T} , respectively. In Fig. 6, we show the condition number $\varpi(\mathbf{T})$ versus a) R_r for $R_d = d\sqrt{\frac{M}{\pi N}} \triangleq R_0$ (cf. (14)) and b) R_d for $R_r = 2d$ assuming $M = 256$, $N = 4$, and different illuminations. As can be seen from Fig. 6 a), for FI and PI, the condition number of \mathbf{T} improves (i.e., decreases) as R_r increases, and for the practical regime $R_r \gg d$, it is close to one. Whereas for SI, the condition number of \mathbf{T} is close to one for the entire considered range of R_r . On the other hand, Fig. 6 b) shows that, for FI and PI, the condition number of \mathbf{T} generally increases (ignoring the side lobes) as R_d increases which is expected since the columns of matrix \mathbf{T} become more similar. Interestingly for SI, the condition number of \mathbf{T} remains again close to one for the entire considered range

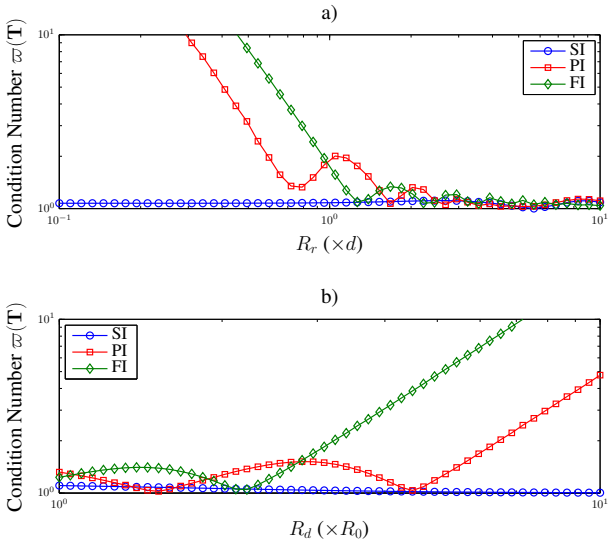


Fig. 6. Condition number $\varpi(\mathbf{T})$ versus a) R_r for $R_d = R_0$ and b) R_d for $R_r = 2d$ assuming $M = 256$, $N = 4$, and different illuminations.

of R_d . From Figs. 5 and 6, we can conclude that SI yields a better performance than PI and FI. More importantly, as far as hardware implementation is concerned, SI is simpler than PI and FI since each active antenna and its respective passive antennas can be manufactured independent of the other active and passive antennas.

C. Comparison of Different MIMO Architectures

For the FD MIMO architecture, we consider the optimal unconstrained precoder obtained from the SVD of the channel and water filling power allocation. For the FC hybrid architecture, we considered the spatially-sparse precoder introduced in [5]. We note that the precoder for the PC architecture can be rewritten as $\mathbf{F} = \mathbf{D}\tilde{\mathbf{T}}\mathbf{D}$ where $\tilde{\mathbf{T}}$ is a fixed matrix whose element in the m -th row and n -th column is one if the m -th antenna is connected to the n -th RF chain and zero otherwise. Therefore, we can apply the proposed precoder design method also to the PC architecture. Finally, we use the AO-based precoder proposed for RA in [16] as a benchmark.

In Fig. 7, we show a) the spectral efficiency R (bits/s/Hz) given in (20), b) the corresponding total consumed power P_{tot} (Watt), and c) the corresponding energy efficiency WR/P_{tot} (bits/joule) versus the number of transmit antennas M for SI, $P_{\text{tx}} = 27$ dBm, $Q = N = 4$, and $J = 16$. As can be seen from Fig. 7 a), the FC hybrid architecture can closely approach the spectral efficiency of the FD architecture. As expected, PC hybrid MIMO has a lower spectral efficiency compared to FC hybrid MIMO due to the fewer degrees of freedom of PC MIMO for beamforming as MN and M phase shifters are used in the FC and PC architectures, respectively. Although the RA and TA architectures have M phase shifters, too, they achieve a slightly lower spectral efficiency compared to the PC architecture due to non-uniform power distribution across the passive antenna elements. Finally, we observe from Fig. 7 a) that the proposed OMP-based precoder outperforms the AO-based precoder in [16] by a large margin. This might be attributed to the fact that the iterative AO-based algorithm

in [16] is more prone to getting trapped in a local optimum which is avoided by the proposed OMP-based precoder which efficiently exploits the sparsity of the mmWave channel. Recall that RA and TA antennas have identical precoder structures as given in (6) but different values of ρ_{ary} which affects their total power consumptions, cf. (10). Therefore, for a given precoder, the spectral efficiencies of RA and TA antennas are identical, cf. Fig. 7 a), whereas their power consumption and energy efficiencies are different, cf. Figs. 7 b) and c).

The main advantage of the RA and TA architectures is their scalability in terms of the number of antennas M which is evident from Figs. 7 b) and c). In fact, RA and TA MIMO (using the proposed precoder) achieve similar performance as FD and FC MIMO if they are equipped with N times more antennas, e.g., in Fig. 7 a), FD and FC MIMO with $M = 256$ antennas and RA and TA MIMO with $M = 1024$ antennas achieve the same spectral efficiency of 29 bits/s/Hz. However, from Fig. 7 b), we observe that the total transmit power of the conventional FD, FC, and PC architectures significantly increases as M increases which makes their implementation quite costly or even infeasible. On the other hand, the total power consumption of the RA and TA architectures stays almost the same as M increases. As a result, we observe in Fig. 7 c) that the energy efficiency of the conventional FD, FC, and PC architectures decreases as M increases whereas the energy efficiency of the proposed RA and TA architectures increases. From Figs. 7 b) and c), we observe that TA antennas have a higher energy efficiency and a lower power consumption compared to RA antennas which is due to the higher array efficiency factor, i.e., $[\rho_{\text{ary}}]_{\text{dB}} = 2[\rho_P]_{\text{dB}} + [\rho_A]_{\text{dB}} = -4.5$ dB and $[\rho_{\text{ary}}]_{\text{dB}} = [\rho_P]_{\text{dB}} + [\rho_A]_{\text{dB}} = -3.5$ dB for RA and TA, respectively, cf. Table II. We note that the sudden jumps in the power consumptions of the FC and PC MIMO architectures in Fig. 7 b) are due to an increase of the number of required GCAs per antenna, i.e., $\lceil \frac{L_{\text{rf}}}{G_{\text{amp}}} \rceil$, as M increases.

Finally, in Fig. 8, we compare the performance of the AO-based precoder in [16] and the proposed OMP-based precoder in more detail for different scattering environments and different numbers of transmit and receive antennas. In particular, in Fig. 8, we show the spectral efficiency (bits/s/Hz) versus the number of channel paths L for SI, $P_{\text{tx}} = 27$ dBm, $Q = N = 4$, $M \in \{400, 1024\}$, and $J \in \{16, 36\}$. From this figure, we observe that as the number of channel paths L increases, the spectral efficiency of the proposed OMP-based precoder first increases and then decreases. This behavior is due to the fact that the proposed OMP-based precoder tries to approximate the optimal unconstrained precoder by selecting the best N paths. Therefore, by increasing L , we have more paths to select from, which yields a diversity gain, but the accuracy of the approximation decreases since N is fixed. In contrast, the spectral efficiency of the AO-based precoder in [16] increases as L increases. This is due to the fact that the AO-based precoder in [16] does not explicitly choose its analog precoder based on the transmit array response of the available paths. In fact, increasing L leads to a better conditioned channel matrix which improves the convergence behavior of this precoder. In addition, we observe from Fig. 8 that the performance gain of the proposed precoder over the AO-based precoder increases with the number of transmit and receive antennas. This behavior

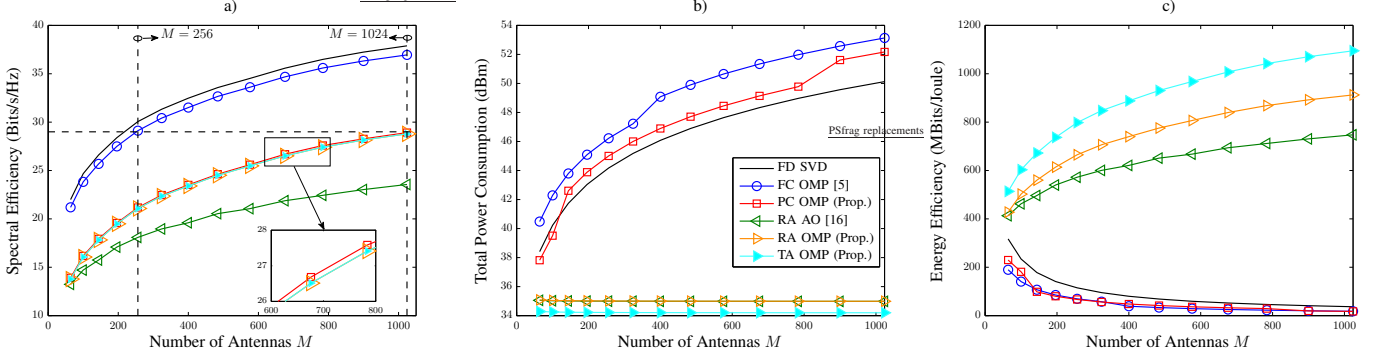


Fig. 7. a) Spectral efficiency (bits/s/Hz), b) total consumed power P_{tot} (Watt), and c) energy efficiency (MBits/Joule) versus number of transmit antennas M for SI, $P_{\text{tx}} = 27$ dBm, $Q = N = 4$, and $J = 16$.

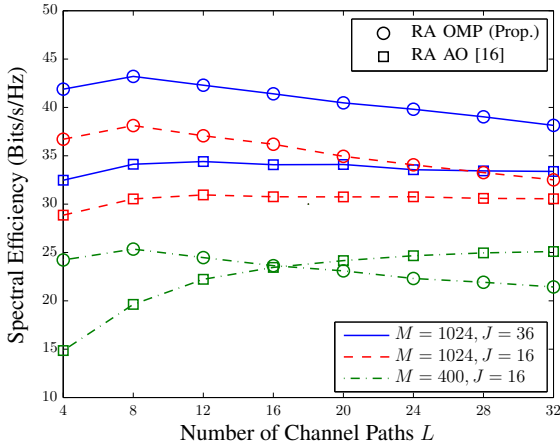


Fig. 8. Spectral efficiency (bits/s/Hz) versus number of channel paths L for SI, $P_{\text{tx}} = 27$ dBm, $Q = N = 4$, $M \in \{400, 1024\}$, and $J \in \{16, 36\}$.

is in line with the results reported in the literature which state that for large M , the optimal unconstrained precoder transmits the data over at most the N strongest channel paths [5], [7].

VI. CONCLUSIONS AND FUTURE WORK

In this paper, we proposed to employ RA and TA architectures to realize the potential of *massive* MIMO in practice. In particular, we first analyzed the corresponding precoder structure and consumed powers. Then, we showed that the precoders for RA and TA antennas have to meet different constraints compared to the precoders for conventional MIMO architectures. Taking these constraints into account and exploiting the sparsity of mmWave channels, we designed two efficient precoders for RA and TA antennas; namely MI- and OMP-based precoders. Furthermore, in order to conduct a fair comparison between the performance of RA and TA antennas with that of conventional FD, hybrid FC, and hybrid PC MIMO architectures, we developed a unified power consumption model. Finally, we presented comprehensive simulation results which revealed several interesting insights for system design. Specifically, we showed that a careful design of the RA and TA antenna architectures leads to a considerable performance improvement. In particular, the distances among the active antennas, respectively, and between the active and passive antennas should be optimized. Interestingly, although SI is preferable for hardware

implementation compared to PI and FI, with the proposed OMP-based precoder, it also yields a better performance. In addition, our simulation results revealed that unlike conventional MIMO architectures, the RA and TA MIMO architectures are highly energy efficient and fully scalable in terms of the number of transmit antennas.

In this paper, we assumed that the transmitter employs RA or TA antenna and we focused on the problem of precoder design assuming an FD receiver. If the number of receive antenna is large, implementing an FD receiver becomes infeasible. An interesting future work is to consider the case where the receiver is also equipped with RA or TA antennas, and to jointly optimize the precoder at the transmitter and the combiner at the receiver, see [5] for a similar design for FD hybrid MIMO. In addition, in this paper, we considered a point-to-point MIMO system, which is a suitable model for e.g. data backhauling from a macro base station (BS) to a small-cell BS. Other interesting practical network architectures include the uplink and the downlink between a BS and multiple mobile users. The design of corresponding precoders and combiners when the BS employs RA or TA antennas constitutes an interesting research problem for future work, see [22] for a similar design for FD hybrid MIMO.

APPENDIX A PROOF OF PROPOSITION 1

Let us define $\bar{\mathbf{x}} = [\bar{x}_1, \dots, \bar{x}_N]^T \in \mathbb{C}^{N \times 1}$ and $\bar{\mathbf{y}} = [\bar{y}_1, \dots, \bar{y}_M]^T \in \mathbb{C}^{M \times 1}$ where \bar{x}_n and \bar{y}_m denote the signal transmitted by the n -th active antenna and the signal received at the m -th passive antenna, respectively. As can be seen from Fig. 1, the data stream vector \mathbf{s} is multiplied by the baseband precoder \mathbf{B} , fed to the RF chains, and then transmitted over the active antennas/illuminators, i.e., $\bar{\mathbf{x}} = \sqrt{P_{\text{tx}}} \mathbf{B} \mathbf{s}$. Let us assume $r_{m,n} \gg \lambda$ such that the passive antennas are in the far field w.r.t. the active antennas. Thereby, the signal that is received at the m -th passive antenna, \bar{y}_m , is obtained as [14]

$$\bar{y}_m = \sum_{n=1}^N \sqrt{P_{\text{tx}} G(\theta_{m,n}, \phi_{m,n})} \frac{\lambda}{4\pi r_{m,n}} e^{-j \frac{2\pi r_{m,n}}{\lambda}} \bar{x}_n. \quad (33)$$

Defining matrix \mathbf{T} in (8), we obtain $\bar{\mathbf{y}} = \mathbf{T} \bar{\mathbf{x}}$. At the passive antenna array, the received signal at the m -th antenna is delayed by phase $2\pi\beta_m$ and reflected/transmitted. Defining \mathbf{D} in (7), we obtain $\mathbf{x} = \mathbf{D} \bar{\mathbf{y}}$. We further note that the signal attenuation due

the aperture efficiency and phase shifter efficiency is captured by the efficiency factor ρ_{ary} , which is included in \mathbf{T} , see Section III-A2. Taking into account ρ_{ary} and considering (4), the precoder matrix can be written as $\mathbf{F} = \mathbf{DTB}$ which is given in (6). This concludes the proof.

APPENDIX B PROOF OF LEMMA 2

Let us define $\tilde{\mathbf{B}} = (\mathbf{C}_1^H \mathbf{C}_1)^{\frac{1}{2}} \mathbf{B} \in \mathbb{C}^{Q \times N}$. Assuming $\mathbf{C}_1^H \mathbf{C}_1$ is a non-singular matrix, the constraint in (24) is rewritten as

$$\begin{aligned} & \text{trace}(\mathbf{C}_1 \mathbf{B} \mathbf{B}^H \mathbf{C}_1^H) \quad (34) \\ &= \text{trace}\left(\mathbf{C}_1 (\mathbf{C}_1^H \mathbf{C}_1)^{-\frac{1}{2}} \tilde{\mathbf{B}} \tilde{\mathbf{B}}^H (\mathbf{C}_1^H \mathbf{C}_1)^{-\frac{1}{2}} \mathbf{C}_1^H\right) \\ &\stackrel{(a)}{=} \text{trace}\left(\tilde{\mathbf{B}} \tilde{\mathbf{B}}^H (\mathbf{C}_1^H \mathbf{C}_1)^{-\frac{1}{2}} \mathbf{C}_1^H \mathbf{C}_1 (\mathbf{C}_1^H \mathbf{C}_1)^{-\frac{1}{2}}\right) = \text{trace}(\tilde{\mathbf{B}} \tilde{\mathbf{B}}^H), \end{aligned}$$

where for equality (a), we used the relation $\text{trace}(\mathbf{XY}) = \text{trace}(\mathbf{YX})$ for $\mathbf{X} \in \mathbb{C}^{n \times m}$ and $\mathbf{Y} \in \mathbb{C}^{m \times n}$. Based on this result and using the definition $\tilde{\mathbf{H}} = \mathbf{H} \mathbf{C}_1 (\mathbf{C}_1^H \mathbf{C}_1)^{-\frac{1}{2}} \in \mathbb{C}^{J \times N}$, the problem in (24) is rewritten as

$$\begin{aligned} & \underset{\tilde{\mathbf{B}} \in \mathbb{C}^{N \times Q}}{\text{maximize}} \left| \mathbf{I}_J + \gamma \tilde{\mathbf{H}} \tilde{\mathbf{B}} \tilde{\mathbf{B}}^H \tilde{\mathbf{H}}^H \right| \\ & \text{C1: } \text{trace}(\tilde{\mathbf{B}} \tilde{\mathbf{B}}^H) \leq 1, \quad (35) \end{aligned}$$

The above problem has the form of MI maximization for an FD MIMO system with equivalent channel matrix $\tilde{\mathbf{H}}$. Thus, the solution is found via the waterfilling algorithm as $\tilde{\mathbf{B}} = [\mathbf{v}_1, \dots, \mathbf{v}_Q] \mathbf{Z}$ [7]. Then, the optimal baseband precoder is given by $\mathbf{B} = (\mathbf{C}_1^H \mathbf{C}_1)^{-\frac{1}{2}} \tilde{\mathbf{B}}$ which concludes the proof.

REFERENCES

- [1] V. Jamali, A. M. Tulino, G. Fischer, R. Müller, and R. Schober, "Scalable and Energy-Efficient Millimeter Massive MIMO Architectures: Reflect-Array and Transmit-Array Antennas," *accepted for presentation at IEEE ICC*, 2019.
- [2] X. Gao, L. Dai, and A. M. Sayeed, "Low RF-Complexity Technologies to Enable Millimeter-Wave MIMO with Large Antenna Array for 5G Wireless Communications," *IEEE Commun. Mag.*, vol. 56, no. 4, pp. 211–217, Apr. 2018.
- [3] I. Ahmed, H. Khammari, A. Shahid, A. Musa, K. S. Kim, E. De Poorter, and I. Moerman, "A Survey on Hybrid Beamforming Techniques in 5G: Architecture and System Model Perspectives," *IEEE Commun. Surveys & Tutorials*, Fourthquarter 2018.
- [4] A. V. Delgado, M. Sanchez-Fernandez, J. Llorca, and A. Tulino, "Feasible Transmission Strategies for Downlink MIMO in Sparse Millimeter-Wave Channels," *IEEE Commun. Mag.*, vol. 56, no. 7, pp. 49–55, Jul. 2018.
- [5] O. El Ayach, S. Rajagopal, S. Abu-Surra, Z. Pi, and R. W. Heath, "Spatially Sparse Precoding in Millimeter Wave MIMO Systems," *IEEE Trans. Wireless Commun.*, vol. 13, no. 3, pp. 1499–1513, Mar. 2014.
- [6] A. F. Molisch, V. V. Ratnam, S. Han, Z. Li, S. Le, H. Nguyen, L. Li, and K. Haneda, "Hybrid Beamforming for Massive MIMO: A Survey," *IEEE Commun. Mag.*, vol. 55, no. 9, pp. 134–141, Sep. 2017.
- [7] R. Ghanaaatian, V. Jamali, A. Burg, and R. Schober, "Feedback-Aware Precoding for Millimeter Wave Massive MIMO Systems," *arXiv*, 2019. [Online]. Available: preprint:1811.04138
- [8] H. Yan, S. Ramesh, T. Gallagher, C. Ling, and D. Cabric, "Performance, Power, and Area Design Trade-offs in Millimeter-Wave Transmitter Beamforming Architectures," *Accepted for publication in IEEE Circuits Syst. Mag.*, 2018. [Online]. Available: <https://arxiv.org/abs/1807.07201>
- [9] X. Gao, L. Dai, S. Han, I. Chih-Lin, and R. W. Heath, "Energy-Efficient Hybrid Analog and Digital Precoding for mmWave MIMO Systems with Large Antenna Arrays," *IEEE J. Select. Areas Commun.*, vol. 34, no. 4, pp. 998–1009, Apr. 2016.
- [10] D. Berry, R. Malech, and W. Kennedy, "The Reflectarray Antenna," *IEEE Trans. Antennas Propag.*, vol. 11, no. 6, pp. 645–651, Nov. 1963.
- [11] D. M. Pozar, S. D. Targonski, and H. Syrigos, "Design of Millimeter Wave Microstrip Reflectarrays," *IEEE Trans. Antennas Propag.*, vol. 45, no. 2, pp. 287–296, Feb. 1997.
- [12] Z. Popovic and A. Mortazawi, "Quasi-Optical Transmit/Receive Front Ends," *IEEE Trans. Microw. Theory Tech.*, vol. 46, no. 11, pp. 1964–1975, Nov. 1998.
- [13] J. Y. Lau, "Reconfigurable Transmitarray Antennas," Ph.D. dissertation, University of Toronto, 2012.
- [14] L. Di Palma, "Reconfigurable Transmitarray Antennas at Millimeter-Wave Frequencies," Ph.D. dissertation, University of Rennes, 2015.
- [15] A. H. Abdelrahman, F. Yang, A. Z. Elsherbeni, and P. Nayeri, "Analysis and Design of Transmitarray Antennas," *Synthesis Lectures on Antennas*, vol. 6, no. 1, pp. 1–175, 2017.
- [16] Z. Zhou, N. Ge, Z. Wang, and S. Chen, "Hardware-Efficient Hybrid Precoding for Millimeter Wave Systems With Multi-Feed Reflectarrays," *IEEE Access*, vol. 6, pp. 6795–6806, 2018.
- [17] C. Liaskos, S. Nie, A. Tsoliaridou, A. Pitsillides, S. Ioannidis, and I. Akyildiz, "A New Wireless Communication Paradigm through Software-controlled Metasurfaces," *arXiv preprint arXiv:1806.01792*, 2018.
- [18] —, "A Novel Communication Paradigm for High Capacity and Security via Programmable Indoor Wireless Environments in Next Generation Wireless Systems," *Ad Hoc Netw.*, vol. 87, pp. 1–16, 2019.
- [19] Q. Wu and R. Zhang, "Intelligent Reflecting Surface Enhanced Wireless Network via Joint Active and Passive Beamforming," *arXiv preprint arXiv:1810.03961*, 2018.
- [20] F. C. Commission, "Use of Spectrum Bands Above 24 GHz For Mobile Radio Services," *Fed. Regist.*, vol. 81, no. 164, pp. 58 270–58 308, 2016.
- [21] G. Fischer, "Next-Generation base Station Radio Frequency Architecture," *Bell Labs Tech. J.*, vol. 12, no. 2, pp. 3–18, Summer 2007.
- [22] C. Lin and G. Y. Li, "Energy-Efficient Design of Indoor mmWave and Sub-THz Systems with Antenna Arrays," *IEEE Trans. Wireless Commun.*, vol. 15, no. 7, pp. 4660–4672, Jul. 2016.
- [23] A. Garcia-Rodriguez, V. Venkateswaran, P. Rulikowski, and C. Masouros, "Hybrid Analog-Digital Precoding Revisited Under Realistic RF Modeling," *IEEE Wireless Commun. Lett.*, vol. 5, no. 5, pp. 528–531, Oct. 2016.
- [24] L. N. Ribeiro, S. Schwarz, M. Rupp, and A. L. de Almeida, "Energy Efficiency of mmWave Massive MIMO Precoding with Low-Resolution DACs," *IEEE J. Sel. Topics Signal Process.*, vol. 12, no. 2, pp. 298–312, May 2018.
- [25] C. A. Balanis, "Antenna Theory, Analysis and Design," 1982.
- [26] B. Sklar, *Digital Communications*. Prentice Hall Upper Saddle River, 2001, vol. 2.
- [27] D. M. Pozar, *Microwave Engineering*. John Wiley & Sons, 2009.
- [28] X. Yu, J.-C. Shen, J. Zhang, and K. B. Letaief, "Alternating Minimization Algorithms for Hybrid Precoding in Millimeter Wave MIMO Systems," *IEEE J. Sel. Topics Signal Process.*, vol. 10, no. 3, pp. 485–500, Apr. 2016.
- [29] A. Alkhateeb and R. W. Heath, "Frequency Selective Hybrid Precoding for Limited Feedback Millimeter Wave Systems," *IEEE Trans. Commun.*, vol. 64, no. 5, pp. 1801–1818, May 2016.
- [30] M. A. Sedaghat, V. I. Barousis, R. R. Müller, and C. B. Papadias, "Load Modulated Arrays: A Low-Complexity Antenna," *IEEE Commun. Mag.*, vol. 54, no. 3, pp. 46–52, Mar. 2016.
- [31] A. K. Khandani, "Media-Based Modulation: A New Approach to Wireless Transmission," in *ISIT*, Jul. 2013, pp. 3050–3054.
- [32] G. H. Golub and C. F. Van Loan, *Matrix Computations*. JHU Press, 2012, vol. 3.